Study the effect of anti-vibration edge length on process stability of milling thin-walled Ti-6Al-4V alloy

Mengyu Li[1] · Wei Zhao[1] · Liang Li[1] · Ning He[1] · Muhammad Jamil[1]

Abstract

Owing to limited rigidity and wall thickness, the machining of thin-walled components leads to chatter, poor surface quality, and low productivity. It is well-acknowledged that end-mill geometry and cutting conditions have a significant influence on the process stability of thin-walled parts. In order to reduce the milling chatter, an anti-vibration milling tool with an anti-vibration edge (60, 90, 120μm) on the flank face is proposed based on the analysis of the process damping effect. The dynamic modeling, numerical computation, and confirmatory experimental analysis are carried out to investigate the effect of anti-vibration edge length on the milling stability of thin-walled titanium-alloy components. The computation results have shown a stable and gradual increase in stable depth-of-cut with the increase of anti-vibration edge length at constant spindle speed. The ultimate stable axial depth increases with the increase of the anti-vibration edge. Besides, the increase of spindle speed reduced the interference between the flank surface of the milling tool and the workpiece due to the decrease of curvature of the vibration mark on the workpiece surface. At higher cutting speed, the relationship between the stability axial depth and anti-vibration edge length reduced. The comparison of computational and experimental results indicate that the anti-vibration edge improved the process damping effect at low cutting speeds, and 120μm anti-vibration edge is optimum to manufacture the flank face of the tools.

1 Introduction

Thin-walled titanium components have been widely used in the aviation and aerospace industry owing to high specific strength, low weight, strong heat, and corrosion resistance. However, due to the hard-to-cut feature of titanium alloy and low rigidity of the thin-walled structure, it is difficult to machining thin-walled titanium components and chatter is easy to occur during the process that restrict the achievement of high product quality and productivity in the aviation industry [1, 2]. In the factory, the cutting speed of machining such materials is very low because of the high cutting speed leading to excessive wear results in tool failure. When the tooth passing frequency is much lower than the chatter frequency, the ultimate stable axial cutting depth at low speed is often greater

than the predicted value that is why the process of damping plays an important role in machining stability [3, 4]. Therefore, it is meaningful to explore the optimum axial depth under the appropriate cutting speed considering the process damping for milling titanium alloys.

The process damping force is generated by the interference between the tool flank face and the workpiece surface which is opposite to the vibration velocity [5]. With the oscillations appearing in a signal tool revolution, the effective clearance angle becomes negative, and the interference occurs [6, 7]. Wu found a linear relationship between the normal damping force and the interference volume between the tool flank face and the workpiece surface and modeled process damping force [8]. This model involved the calculation of pressure-volume and the process damping force coefficient. Since then, many scholars have carried out the identification of process damping parameters and prediction of cutting stability based on Wu's model. Montgomery and Altintas et al. [9] studied the process damping force mechanism in dynamic milling, and they found that the process damping force was proportional to the yield stress and interference area of the workpiece material. Elbestawi et al. [10] improved Wu's model and

✉ Wei Zhao
  nuaazw@nuaa.edu.cn

1   College of Mechanical and Electrical Engineering, Nanjing
    University of Aeronautics and Astronautics, Nanjing 210016, China

extended the process damping force model based on the relationship between the clearance angle and the slope of the surface ripple. This model is suitable for a tool that is blunt and its wear is known. They also analyzed the machining stability under vertical milling conditions, and successfully predicted the phenomenon of improved cutting stability under low speed. Chiou et al. [11] and Liang et al. [12] mentioned the wear state as the wear belt length at the tip and edge of the cutting tool. Under the assumption of a small vibration value, the pressing volume is calculated analytically to simplify Wu's nonlinear pressing model [8] into a linear viscous damping model. Budak and Tunc [13] used the law of energy consumption equilibrium. They concluded that energy consumed by the process damping force is equal to the energy consumed by the equivalent line viscous damping. Thus, the process damping is equivalent to the linear viscous damping, and the energy consumption equivalent process effectively solves the nonlinear problem of the process damping. Ahmadi [14] obtained stability lobes based on a nonlinear process damping model. It was observed the amplitude of the ultimate stable cycle by an average method and found an analytical relationship between the stability lobe diagram and the amplitude of the ultimate stable cycle. Tuysuz and Altinas [15] predicted the stability of the five-axis ball milling impeller blade practically considering the cutting edge geometry, cutting conditions, material characteristics, and surface ripple characteristics of the workpiece. Sims and Turner [16] introduced a nonlinear process damping force model using the contact length on the tool flank face and revealed the relationship between the feed rate and the damping wavelength of the process. Bachrathy and Stepan [17] presented a milling process damping model considering the tool wear band, and obtained the stability lobes with the semi-discretization method. They also explored the influence of different widths of the tool wear band on the stability lobes. Cao et al. [18] proposed an energy dissipation principle to relate the flank wave indentation area to process damping coefficients. Analytical and numerical integration method was used to establish stability lobes, and the time for calculating was greatly reduced.

The above literature concludes that the higher stable cutting depth can be achieved under the effect of process damping, and high-efficiency cutting can be achieved at low speeds. This could be important to increase the machining productivity of titanium alloy. Besides, the process damping effect is related to the interference area, clearance angle, and the shape of the flank face. It is mentioned previously [2] that a small clearance angle and blunt circular flank face can increase the interference volume of the tool/workpiece, and ultimately increase the machining stability. The micro-chamfering edge ground on the flank face forms a micro anti-vibration edge, which increases the process damping effect by increasing the interference area between the flank face and the workpiece surface. The chatter can be suppressed with the use of a micro-chamfering edge tool in

the machining process. To investigate their effects, the anti-vibration tool with a micro-chamfering edge on the flank surface is designed. Compared with other tool structures such as the blunt circular flank face, the micro-chamfering edge is easier to be realized. Besides, the influence of the length of tool anti-vibration edge on the stability of milling thin-walled titanium alloy parts is also studied with numerical simulation. At last, the milling experiments were carried out to verify the effectiveness of the anti-vibration tool.

2 Milling dynamic model

The workpiece to be machined is titanium alloy thin-walled parts. To simplify the model, a large-diameter solid carbide end mill is selected to ensure that the tool's stiffness is much greater than the workpiece's stiffness. In this case, the tool in the tool-workpiece system is a rigid piece, and the workpiece is a flexible piece. So, only the vibration of the workpiece is considered in the machining process; the model can be simplified as Fig. 1.

The natural coordinate system XOY is established. Since the stiffness in the X-direction is much larger than the Y-direction, therefore, only the cutting force in the Y-direction is considered. The angular position ϕ_j of the jth cutting tooth at each axial level z is:

$$\phi_j(z) = \theta + (j-1)\frac{2\pi}{N} - \frac{z\tan(\beta)}{R} \qquad j = 1 : N \qquad (1)$$

where β is the helix angle, N is the total number of teeth, and R is the tool diameter. θ, calculates from the equation ($\theta = \omega t$, ω is the angular speed), is the angular position of tool bottom (axial level $z = 0$).
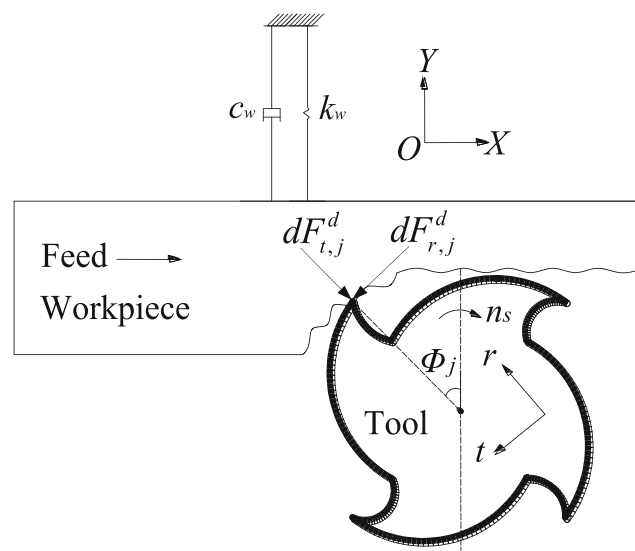

Fig. 1 Milling of titanium alloy thin-walled parts

Because the static cutting thickness does not affect the change of dynamic cutting force, only the dynamic cutting thickness is considered. The instantaneous cutting thickness of the jth cutting tooth at the height z and time t is:

$$h_j(\text{t}, \text{z}) = (y_w(t) - y_w(t - T_j))g(\phi_j(z)) \quad (2)$$

where $y_w(t)$ is the current tooth vibration displacement in the Y-direction, and $y_w(t - T_j)$ is the former tooth vibration displacement, and T is the tooth passing interval.

When angular position $\phi_j < \phi_{st}$, the tool is out of contact with the workpiece, and the cutting force and process damping force are zero. When $\phi_j > \phi_{ex}$, the cutting force is also regarded as zero. The unit step function which determines whether the tooth is in or out of the cutting; g is always defined as 1 when $\phi_j \in (\phi_{st}, \phi_{ex})$; otherwise, g is 0. In consideration of the helix angle of the tool, the scope of g should be expanded. In the paper, the definition of g is:

$$\begin{cases} g(\phi_j(z)) = 0 & \theta < \phi_{st} \text{ or } \theta > \phi_{ex} + \dfrac{a_p}{R}\tan(\beta) \\ g(\phi_j(z)) = 1 & \phi_{st} < \theta < \phi_{ex} + \dfrac{a_p}{R}\tan(\beta) \end{cases} \quad (3)$$

where a_p is axial cutting depth. In down milling, $\phi_{st} = \pi$ and ϕ_{ex} is:

$$\phi_{ex} = arccos\left(\frac{a_e - R}{R}\right) \quad (4)$$

where a_e is the radial depth.

The dynamic cutting force is modeled using the linear edge force model, where elemental tangential and radial forces, F_t and F_r on tooth j, are proportional to the cutting force coefficients (K_{tc}, K_{rc}) and instantaneous chip thickness (h) and differential axial depth of the cut dz:

$$\begin{cases} dF_{t,j}(t, z) = K_{tc}h_j(\phi_j(z))dz \\ dF_{r,j}(t, z) = K_{rc}h_j(\phi_j(z))dz \end{cases} \quad (5)$$

The differential cutting forces are then resolved in Y-directions:

$$dF_{y,j}(t, z) = dF_{t,j}(t, z)\sin(\phi_j(z)) - dF_{r,j}(t, z)\cos(\phi_j(z)) \quad (6)$$

According to Wu's classic process damping force model [8], for the jth tool tooth, differential indentation forces (process damping force) acting on the axial level z, in normal dF_v^d and dF_f^d in frictional directions, are given as:

$$\begin{cases} dF_{v,j}^d(t, z) = K^d S_j(t, z)dz \\ dF_{f,j}^d(t, z) = \mu dF_{v,j}^d(t, z) \end{cases} \quad (7)$$

where $S_j(t, z)$ is the interference area between the tool flank face and the workpiece surface at axial level z (Fig. 2), which is calculated by the method provided in the Appendix 1.

μ is the coefficient of contact friction; K^d is the indentation coefficient. The process damping force in r and t direction can be expressed in terms of the force in v direction and the friction coefficient μ.

$$\begin{cases} dF_{r,j}^d(t, z) = dF_{v,j}^d(t, z)(cos(\alpha) + \mu sin(\alpha)) \\ dF_{t,j}^d(t, z) = dF_{v,j}^d(t, z)(-sin(\alpha) + \mu cos(\alpha)) \end{cases} \quad (8)$$

The differential process damping force is then oriented in Y-direction using the damping force in r and t directions as follows:

$$dF_{y,j}^d(t, z) = dF_{t,j}^d(t, z)sin(\phi_j(z)) - dF_{r,j}^d(t, z)cos(\phi_j(z)) \quad (9)$$

Thus, the equations of milling dynamic can be generated; it should be mentioned that the direction of cutting force exerted on the workpiece is opposite to the forces exerted on the tool:

$$m_y\ddot{y}_w + c_y\dot{y}_w + k_y\ddot{y}_w = -g(\phi_j(z)) \sum_{j=1}^{N} \sum_{k=1}^{S} \varphi_r(z)\left(dF_{y,j} + dF_{y,j}^d\right)dz \quad (10)$$

The interference between the edge and the machined surface is a kind of micro phenomenon. The process damping effect is related to the interference area, and the interference area is related to the shape of the tool's flank face. The anti-vibration edge is formed by the micro-chamfering edge is ground on the tool's flank face. It can increase the process damping effect and the milling process stability.

2.1 Statement 1: the effect of anti-vibration edge length on process damping

Figure 3 is used to represent the relative position relationship between the tool and the workpiece surface in the cutting process. The tool interferes with the vibration grain at point B, assuming that there is an interference between the flank face and the machined surface.

Figure 4 shows the tool without an anti-vibration edge on the flank face; there is only one conventional flank face AE, and the interference area between the tool and the machined
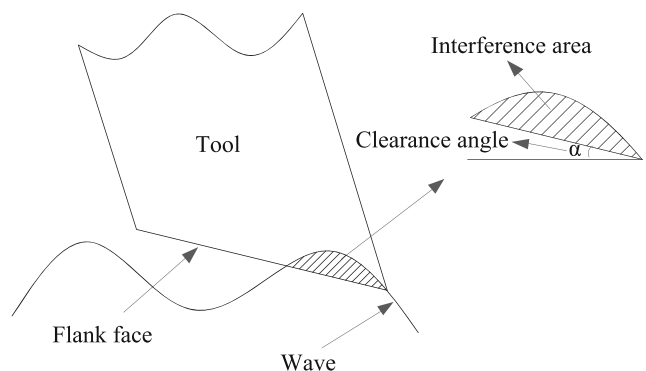

Fig. 2 Interference between flank face and workpiece surface
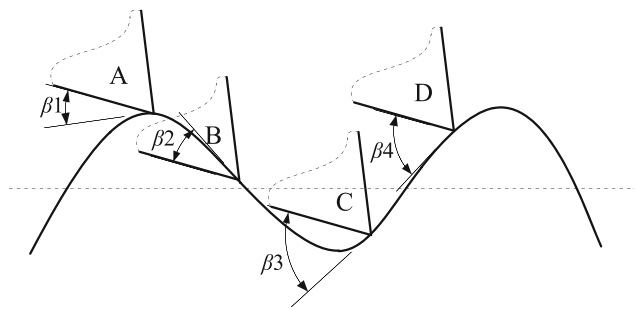
Fig. 3 Relative position relationship between tool and workpiece surface

surface is Sa. While AB is the anti-vibration edge formed on the flank face of the tool, the area of interference increases. By increasing the length of the anti-vibration edge from AB to AC, the interference area increases gradually. Similarly, the length of the anti-vibration edge increases from AB to AD; the increase of the interference area becomes smaller, and until it stops increasing. This phenomenon shows that the anti-vibration edge can increase the area of interference between the flank face and the machined surface. When the speed is constant, and the length of the anti-vibration edge change within a certain range, the interference area increase with the increase of the length of the anti-vibration edge, but growth becoming smaller and eventually stop increase.

2.2 Statement 2: the effect of cutting speed on process damping

Besides, different spindle speeds, the curvature of the vibration marks on the machined surface changes, and the interference between the flank face and machined surface are also different. According to the literature [5], the radial vibration velocity of the tool $\dot{r}$ has the following relationship with the cutting speed ν_c and the clearance angle of the tool α:

$$\dot{r} < \nu_c tan(\alpha) \tag{11}$$

It is known from Eq. (11) and Fig. 5 that if the cutting speed ν_c increase, the curvature of the vibration marks on the machined surface will decrease, and the wavelength of the
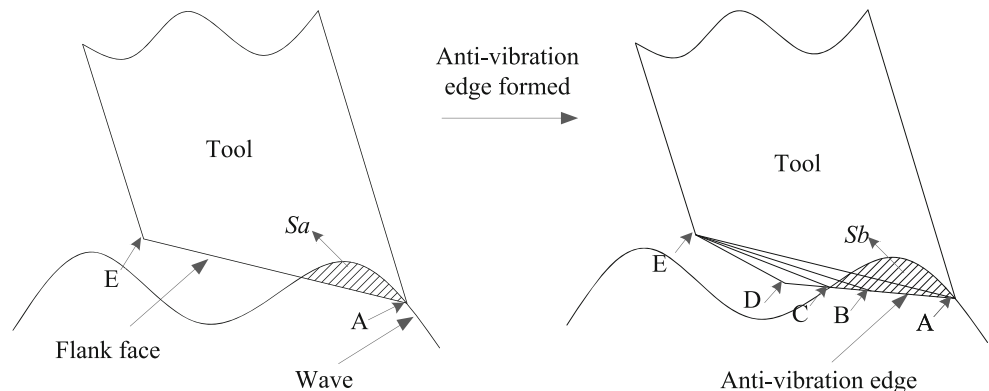
vibration marks will increase. But the interference area between the flank face and machined surface will decrease, the process damping effect is weakened, and the influence of the tool anti-vibration edge on the machining stability is gradually reduced. It means that when the spindle speed reaches a certain value, the process damping effect disappears, and the anti-vibration tools lose its vibration suppression effect.

The main theme of the dynamic modeling is indicating two major claims that increasing the length of the anti-vibration edge increases the process damping effect. This may due to the increasing interference area between the edge and the machined surface. Similarly, increasing the cutting speed decreases the process damping effect. As the curvature of the vibration marks on the machined surface decrease, the interference area decreases the process damping effect. The dynamic model claims have been verified further regarding the computations and experimental findings.

3 Time-domain computation

In order to verify statements 1 and 2, time-domain computations are carried out. In the time domain computations, stability lobe diagrams are determined ultimate stable cutting depth at varying anti-vibration edge length.

3.1 Algorithm design and computations parameters

Equation (10) is solved by the fourth-order Runge-Kutta method, where time increment Δt is 10^{-5} s. The nondimensional chatter parameter, λ, is evaluated as:

$$\lambda = \frac{h_{d,max}}{h_{s,max}} \tag{12}$$

where $h_{d,\,max}$ is the maximum static uncut chip thickness, and $h_{s,\,max}$ is the largest dynamic chip thickness. From the criterion to judge provided in [19], $\lambda=1.25$ is predetermined the limit in this paper. If λ is less than 1.25, the milling process

Fig. 4 The influence of anti-vibration edge length on the interference area

Fig. 5 The influence of cutting speed on the interference area
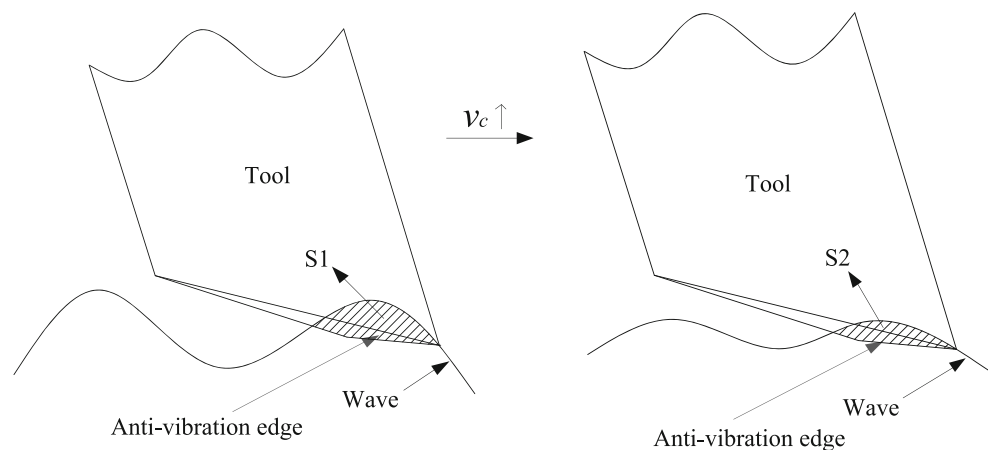
is stable; otherwise, the milling process is unstable. The repeatable execution algorithm is written in Appendix 2.

The natural frequency ω_{ny} =2140Hz, the modal damping ratio of ξ_y=0.031, and the modal stiffness of k_y=4.18 × 10^6 N/m are considered. Besides, during slot milling, the tangential cutting force coefficients K_{tc}=1800Mpa; the radial force coefficient of K_{rc}=600Mpa are determined. The process damping coefficients for titanium alloy Ti6Al4V indentation coefficient is K^d=30,000 N/mm^3; the friction coefficient is μ=0.3, which are obtained from published work [20].

3.2 Stability analysis

According to Section 3.1, MATLAB is used for numerical computations analysis. The length of the axial element is set as 0.2mm, the time step of the single cutter tooth period is 10^{-5}s, and the discrete points of the interference area on the flank face are 100. To ensure more accurate analysis results, the total period is 16T. The computations result at 1000rpm, 1500rpm, and 2000rpm are shown in Fig. 6a, b, and c.

As can be seen from the above three figures, when the length of the anti-vibration edge change in a certain range, the ultimate stable axial cutting depth changes with it. When the spindle speed is 1000r/min, the cutting speed is 50m/min which is a common parameter for cutting titanium alloy. In Fig. 6(a) when the length of the anti-vibration edge changes in the range of 20~120μm, the ultimate stable axial depth increase with the increase of it. And the ultimate stable axial depth increase from 2.2 to 4.6mm. When the length of the anti-vibration edge is greater than 120μm, the ultimate stable axial depth is not changed with the increase of the length of the anti-vibration edge, and it remains 4.6mm. When the spindle speed is 1500r/min, the process damping effect decreases with the cutting speed increases. In Fig. 6(b), when the length of anti-vibration edge changes in the range of 20 to 180μm, the ultimate stable axial depth increases from 1.6 to 3.9mm. If the length of the anti-vibration edge is greater than 180μm, the ultimate stable axial depth will remain constant.

From statement 2, it can be found that, if the cutting speed ν_c increases, the damping effect is weakened, and the influence of the tool anti-vibration edge on the machining stability is gradually reduced. By comparing Fig. 6(a, b), the increments of ultimate stable axial depth decrease with the increase of spindle speed, while the ultimate effective length of the anti-vibration edge increases. When the spindle speed is 1000r/min, the ultimate effective length of the anti-vibration edge is 120μm. However, this value is 180μm when the spindle speed is 1500r/min. When the spindle speed is 2000r/min (the cutting speed is 100m/min), the process damping effect is much weaker than it in Fig. 6(a) and (b), and the stable axial depth increase from 1.4 to 2.8mm with the length of anti-vibration edge increase from 20 to 180μm.

The calculated results are consistent with the previous analysis. The process damping effect is enhanced with the increase of anti-vibration length, and the length of anti-vibration has ultimate value. When the length exceeds the ultimate value, the process damping effect will not be enhanced anymore. Besides, with the increase in cutting speed, the process damping effect is weakened gradually.

## 3.3 Summary of the computations findings

3.3.1 Statement 1

Finding of computation results regarding statement 1, increasing anti-vibration edge length increases the ultimate stable cutting depth. Numerical computations results show that when the length of the anti-vibration edge changes in the range of 20 to 180μm, the ultimate stable axial depth also increases. Under different cutting speeds, the same trend proves the dynamic modeling statement 1.
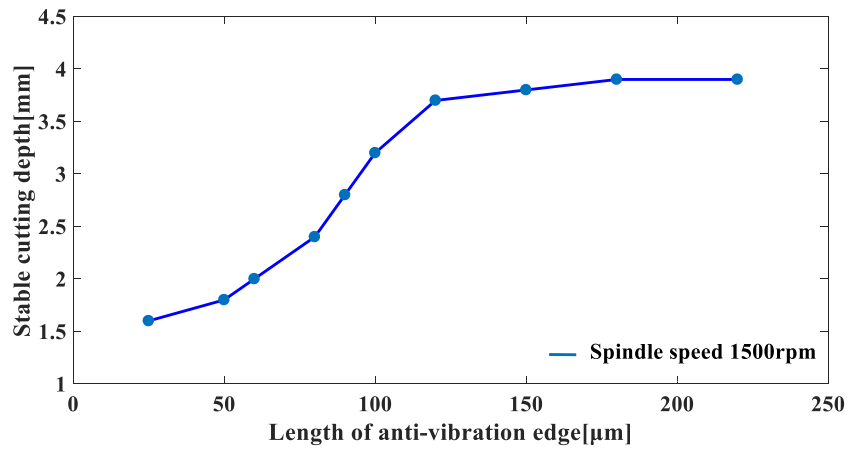
3.3.2 Statement 2

Finding of computation results regarding statement 2, the increments of ultimate stable axial depth decrease
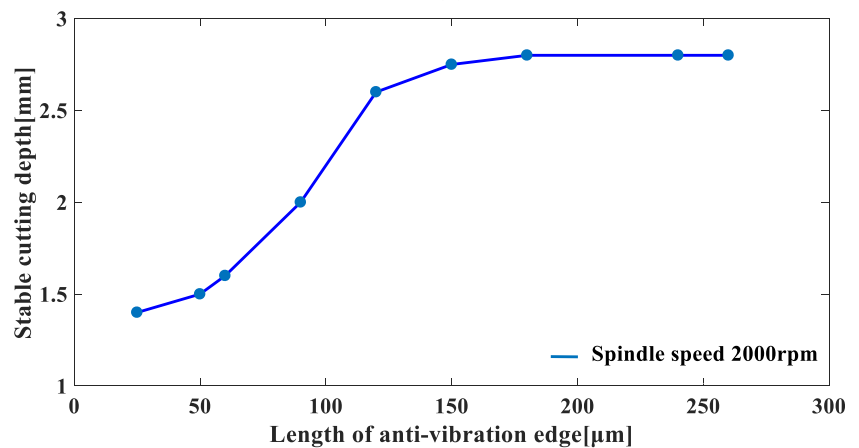
Fig. 6 Stable diagrams with different length of anti-vibration edge. **a** The computational stability limits at 1000rpm; **b** The computational stability limits at 1500rpm; **c** The computational stability limits at 2000rpm
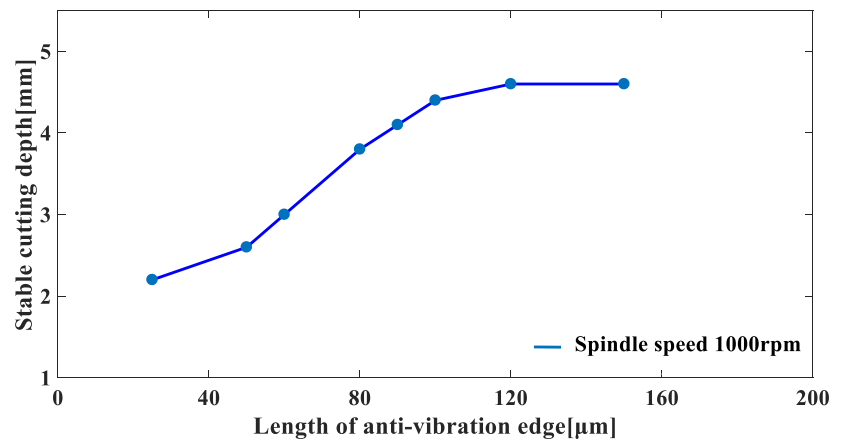
(a)

(b)

(c)

with the increase of spindle speed. Numerical computation results show that when the spindle speed increases from 1000 to 2000rpm, the ultimate stable axial depth decreases. Besides, under the different lengths of anti-vibration edge, the same trend proves the dynamic modeling statement 2.

4 Experimental confirmation

4.1 Experiment equipment

To verify the anti-vibration effect of different tools with anti-vibration edge, the computations and experiments are all
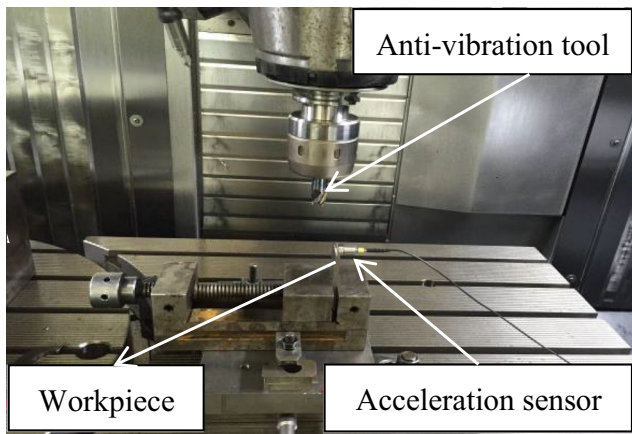
Fig. 7 The milling experiments scenes

achieved. Experiment scenes are shown in Fig. 7, and experimental equipment are as follows: Machine is DMG MORI-DMF 18017, workpiece material is Ti6Al4V (size 40×5×70mm), data acquisition card is NI USB-6218, the piezoelectric acceleration sensor is BW14100 SN-01645.

4.2 Tool geometric parameters (Table 1)

Table 1 Tool parameters

	Tool 1	Tool 2	Tool 3
Tool material	Carbide end mill		
Diameter	16mm		
Tool length	75 mm (35 mm edge length)		
Length of anti-vibration edge	60μm	90μm	120μm
Number of flutes	4 flutes		
Clearance angle	α_1 is 4 °, α_2 is 9 °		
Helix angle	35 °		

4.3 Cutting and model parameters

Main parameters are as follows: radial cutting depth a_e=0.8-mm, feed per tooth f_z=0.06mm/z, down milling, mist cooling (Table 2).

5 Result and discussion

5.1 Stability lobe diagrams under different tool designs

To verify the results of the numerical computations, three types of cutting tools having different anti-vibration edge (60, 90, 120μm) lengths on the flank surface are selected and different parameters are selected (Fig. 8) for experiments. The acceleration sensor that measures the vibration signal is

Table 2 Experiment parameters

Tool design	Sr no.	Spindle speed (r/min)	Axial depth (mm)
Tool 1	A1	1000	2.4
	B1	1000	3.8
	C1	1500	1.6
	D1	1500	2.8
	E1	2000	2.4
Tool 2	A2	1000	3.8
	B2	1000	4.6
	C2	1500	2.2
	D2	1500	3.2
	E2	2000	2.6
Tool 3	A3	1000	4.2
	B3	1000	5.2
	C3	1500	3.2
	D3	1500	4.2
	E3	2000	3.2

stuck to the workpiece, and the acceleration signals are collected during the experiment.

5.2 Acceleration under tool designs

In these experiments, acceleration signals are collected and analyzed by fast Fourier transform, and the partial results are shown in Fig. 9. As chatter frequency is close to the structural natural frequency, and the natural frequency of the workpiece-clamp system is about 2100Hz, so the 1800–2400Hz frequency range is selected for analysis. Figure 9(d, e) shows that when the cutting parameters are selected in the stable area, the milling process mainly appears spindle rotation frequency (record as "□") and tooth pass frequency (record as "○"). However, when the parameters are selected in the unstable area, besides the spindle rotation frequency and tooth pass frequency, chatter frequency appeared (record as "☆") around the workpiece-clamp system natural frequency in Fig. 9a, b, c, and f. The experimental results show a good agreement with the results of the numerical computation, and tools with longer anti-vibration edge lengths show better stability in the milling process. As the cutting speed increase, the effect of anti-vibration edge and ultimate stable axial depth decrease. Statement 1 and 2 are proved fully in the experiment.

5.3 Surface topography under tool designs

After the experiments, the machined surface topography of the workpiece is obtained by a CCD microscope in Fig. 10. The marks left on the machined surface can directly indicate the stable state of the milling process.

Figure 10(a) is the machined surface topography when using tool 3 and selecting A3 cutting parameters; the surface is very smooth and only little straight marks are left. It indicates that the cutting process is stable. Figure 10(b) is the machined surface topography when using tool 2 and selecting B2 cutting parameters. It is found from the surface topography
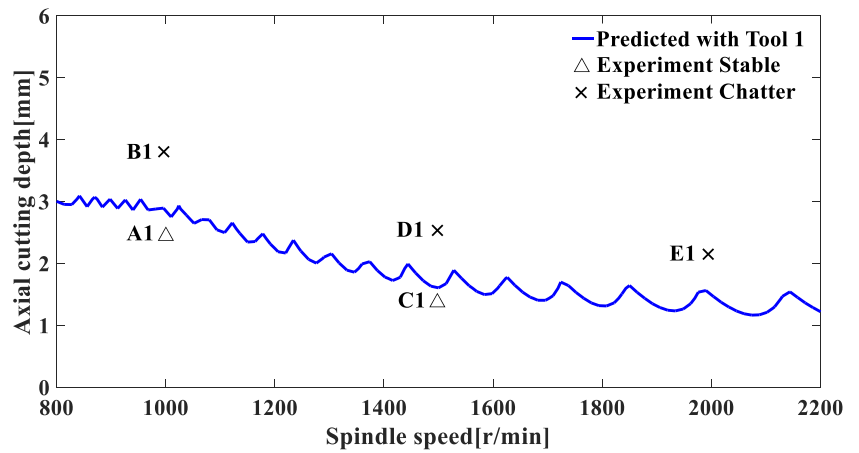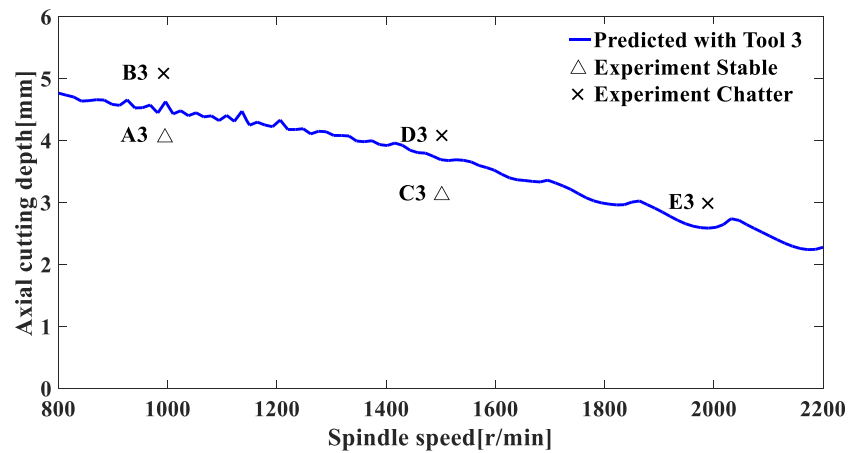
(a)
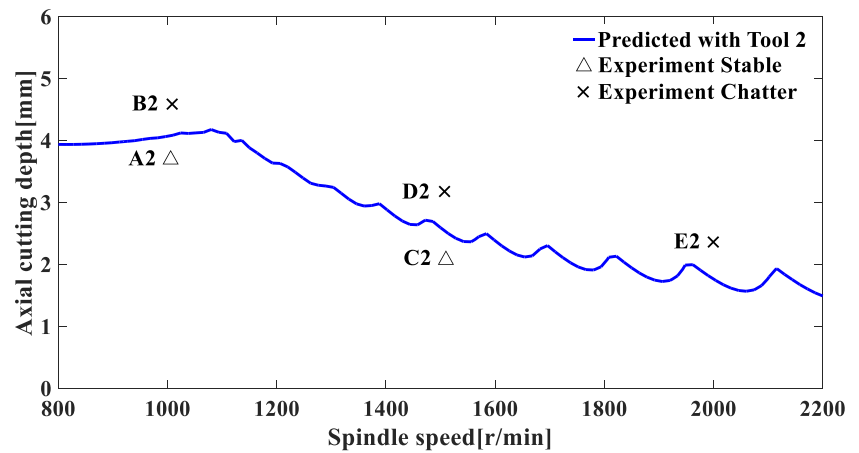
(b)

(c)

that lots of typical oblique chatter marks appear on the work-piece surface, which is a symbol of the occurrence of chatter. Besides, the surface roughness Ra of the workpiece machined in a stable process is 0.229μm, and the workpiece surface roughness is 0.482μm when the milling process is unstable. The occurrence of chatter seriously affects the surface quality.

6 Conclusion

Chatter will restrict the milling efficiency and surface quality of thin-walled titanium alloy parts. In low-speed milling, the process damping effect can be used to consume vibration energy, to suppress chatter. In this paper, the influence of the
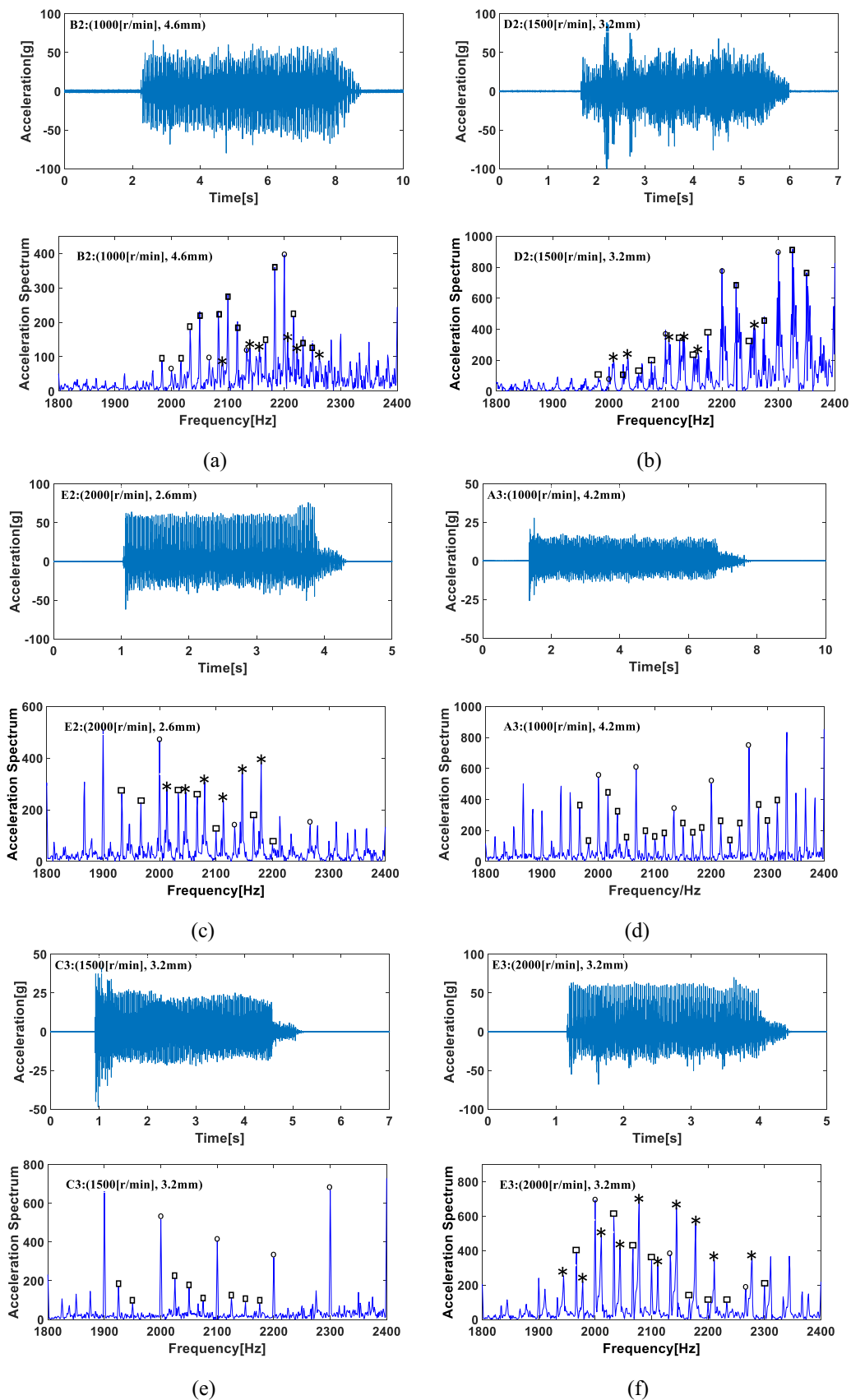
Fig. 9 Spectral analysis result. **a**, **b**, and **c** show the measured acceleration signals and spectral analysis results at experiment point B2, D2, and E2 with tool 2. **d**, **e**, and **f** show the measured acceleration signals and spectral analysis results at experiment point A3, C3, and E3 with tool 3
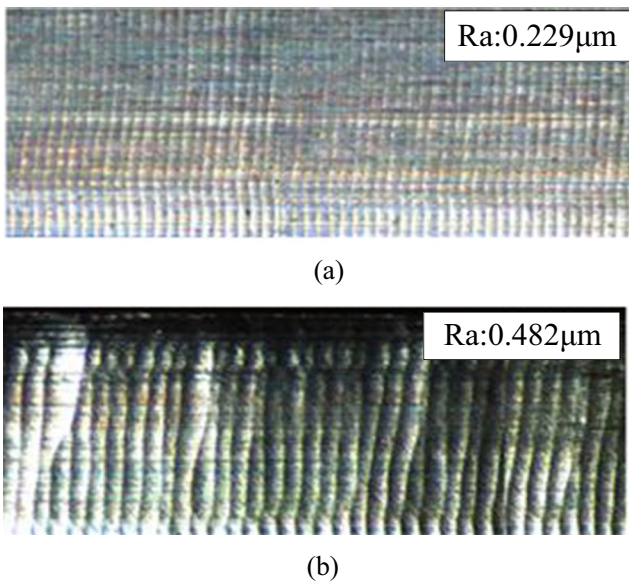
(a)

(b)

Fig. 10 Comparisons of machined surface topography

length of the anti-vibration edge on process damping effect and milling stability is studied, and the numerical computation are carried out utilizing the fourth-order Runge-Kutta method. Finally, cutting tools with three different length of anti-vibration edge are selected for the experiments, and the following conclusions are obtained:

(1) In the low cutting speed region, when the length of the anti-vibration edge changes within a certain range, the ultimate stable axial depth increases with the increase of the length of the anti-vibration edge. When the vibration frequency is unchanged, the lower the speed, the greater the curvature of the vibration marks, the interference is more easily to occur between the flank face and workpiece surface. However, when the length of the anti-vibration edge increases to a certain limit value, the ultimate axial stable depth does not change anymore, and the influence of anti-vibration edge on the milling stability will disappear.

(2) When the cutting speed is too large, the wavelength of surface vibration marks increases, the curvature decreases correspondingly. Also, the interference between the flank face and the workpiece weakens, and the influence of process damping on machining stability decreases or even disappears, so the relationship between the ultimate stable cutting depth and the length of anti-vibration edge loses the general rule.

(3) In the milling of titanium alloy, process damping effect is an effective way to suppress chatter and to ensure the stability of the machining process. In this research, a 120-μm anti-vibration edge is recommended to form on the flank face of the tools. According to the experiment results, anti-vibration tools with anti-vibration edge and clearance angle show good chatter suppressing effect.

Appendix 1
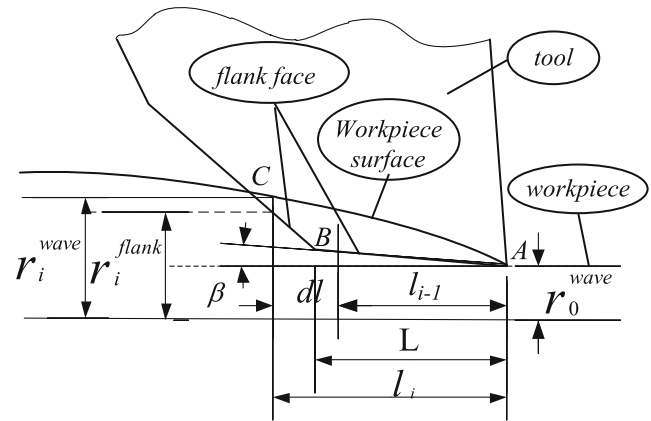
Calculation of indentation area

Fig. 11 The calculation of indentation area

The calculation model of the indentation area $S(t, z)$ at axial level z is shown in Fig. 11, where r_0^{wave} is the current radial coordinate values of the wave, $i(i=2,...,n-1)$ is the time step, L is the length of anti-vibration edge, r_i^{flank} is radial coordinate values on the flank face, r_i^{wave} is radial coordinate values of wave calculated in the previous time, $\beta=4°$ is the anti-vibration clearance angle [5], γ is the conventional clearance angle, and l is indentation length. The indentation area $S(t)$ is bounded by the tool flank face and the workpiece surface wave, and it is calculated at each simulation time-step numerically.

$$\begin{cases} r_i^{flank} = r_0^{wave} + l_i\tan(\beta) & l_i < L \\ r_i^{flank} = r_0^{wave} + l_i\tan(\beta) + (l_i-L)\tan(\gamma-\beta) & l_i > L \end{cases} \quad (13)$$

$$\begin{cases} dS_i = \dfrac{dr_i + dr_{i-1}}{2}dl & i = 2,...,n-1 \\ dS_1 = \dfrac{ddr_1}{2}dl \\ dS_n = \dfrac{dr_{n-1}^2}{2(dr_{n-1}-dr_n)}dl \\ S(t,z) = \sum\limits_{i=1}^{n} dS_i \end{cases} \quad (14)$$

In the Eq. (14):

$$\begin{aligned} dr_i &= r_i^{wave} - r_i^{flank} \\ l_i &= i \cdot dl \end{aligned} \quad (15)$$

Tool and workpiece coordinates can be obtained by the fourth-order Runge-Kutta method. Equation (10) is organized as first-order equations as:

$$y' = f(t,y) \quad (16)$$

where

$$y = \left\{ y_w \ \dot{y}_w \right\}^T$$

$$f = \begin{bmatrix} 0 & 1 \\ -\omega_{ny}^2 & -2\xi_y\omega_{ny} \end{bmatrix} y + \left\{ \begin{matrix} 0 \\ F \end{matrix} \right\}$$

$$F = g(\phi_j(z)) \sum_{k=1}^{S} \varphi_r(z)\left(dF_{y,j} + dF_{y,j}^d\right)/m_y dz \qquad (17)$$

$$m_y = \frac{k_y}{\omega_{ny}^2}$$

$$\begin{cases} y_{i+1} = y_i + \dfrac{h}{6}(k_1 + 2k_2 + 2k_3 + k_4) \\ k_1 = f(t_i, y_i) \\ k_2 = f\left(t_i + \dfrac{1}{2}h, y_i + \dfrac{1}{2}hk_1\right) \\ k_3 = f\left(t_i + \dfrac{1}{2}h, y_i + \dfrac{1}{2}hk_2\right) \\ k_4 = f(t_i + h, y_i + hk_3) \end{cases} \qquad (18)$$

The iterative formula of the tool and workpiece coordinates from the ith time to the $(i+1)$th time is as follows:

Appendix 2

Figure 12 shows the repeatable execution algorithm for time-domain computation. Using the following steps, the computational stability limits are obtained.

Fig. 12 The algorithm of stability chart
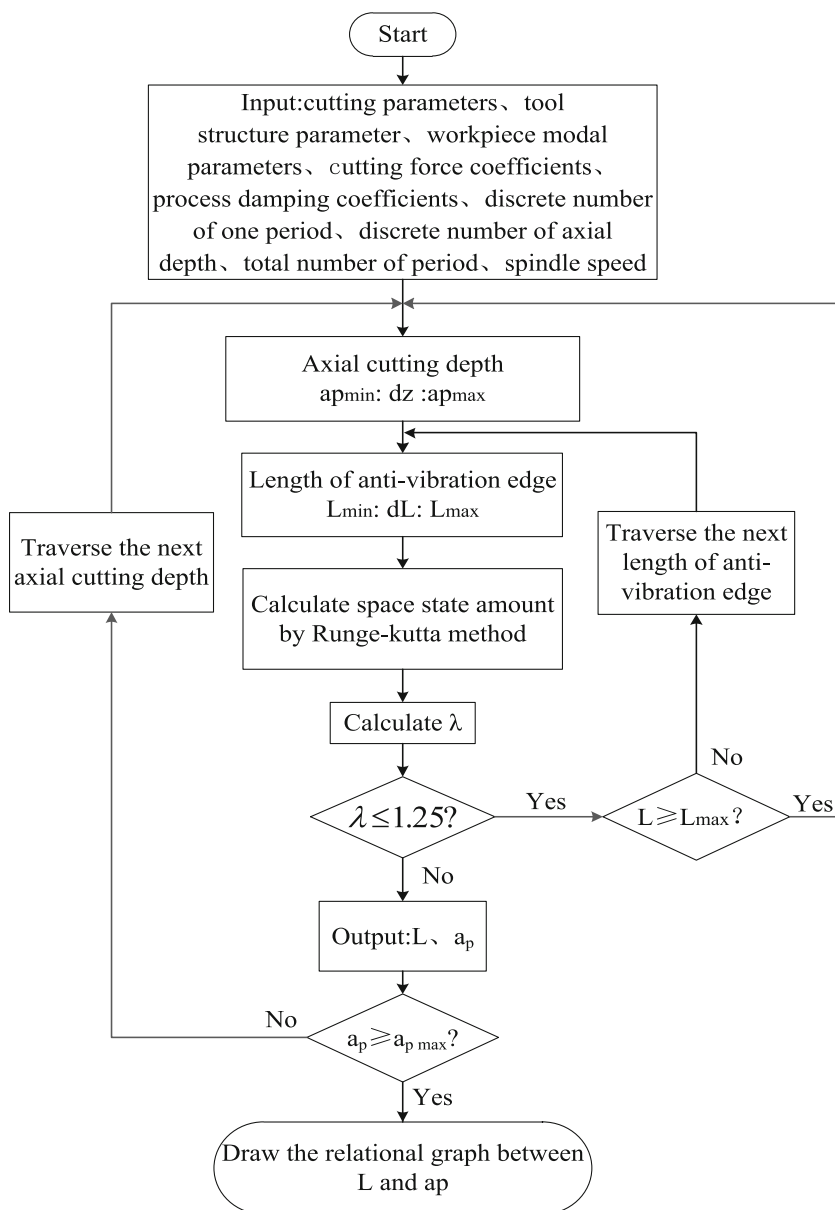
(1) The input parameters are cutting tool geometry, modal parameters, entry angle and exit angle cutting force and process damping coefficients, and the total number of periods.

(2) For a given length of anti-vibration edge, a static time-domain computation is run and the maximum static uncut chip thickness $h_{d, max}$ is stored. Then, a second time-domain computation is run. The vibration displacement and dynamic chip thickness h_s are obtained. The largest dynamic chip thickness of all cutting points on the tool, $h_{s, max}$, is stored for the last few revolutions of the computations. Then, λ is calculated.

(3) If $\lambda < 1.25$, the process is stable, a_{min} is set to the current value of a, a is doubled, and step (2) is repeated until the process is unstable. Then, a_{max} is set to the value of a.

(4) If $\lambda > 1.25$, the process is unstable, a_{max} is set to the current value of a, a is halved, and step (2) is repeated until the process is stable. Then, a_{min} is set to the stable axial cutting depth, a.

Author contribution Conceptualization: ML; methodology: ML, WZ; original draft writing: ML, MJ; investigation: NH, LL; review: WZ, LL; language editing: ML, MJ, WZ; supervision: NH, WZ.

Declarations

Ethics approval and consent to participate   Not applicable.

Consent for publication   The copyright permissions have been taken and consent to submit has been received explicitly from all co-authors.

Competing interests   The authors declare no competing interests.

References

1. Altintas Y, Weck M (2004) Chatter stability of metal cutting and grinding. CIRP Ann 53:619–642. https://doi.org/10.1016/S0007-8506(07)60032-8

2. Li X, Zhao W, Li L, He N, Chi SW (2015) Modeling and application of process damping in milling of thin-walled workpiece made of titanium alloy. Shock Vib 2015:1–12. https://doi.org/10.1155/2015/431476

3. Munoa J, Beudaert X, Dombovari Z, Altintas Y, Budak E, Brecher C, Stepan G (2016) Chatter suppression techniques in metal cutting. CIRP Ann 65:785–808. https://doi.org/10.1016/j.cirp.2016.06.004

4. Sisson TR, Kegg RL (1969) An explanation of low-speed chatter effects. J Eng Ind 91:951–958. https://doi.org/10.1115/1.3591778

5. Li X, Zhao W, Li L, He N (2014) 1363. Modeling, identification and application of process damping in milling of titanium alloy. J Vibroengineering

6. Altintas Y, Eynian M, Onozuka H (2008) Identification of dynamic cutting force coefficients and chatter stability with process damping. CIRP Ann - Manuf Technol. 57:371–374. https://doi.org/10.1016/j.cirp.2008.03.048

7. Tlusty J (1978) Analysis of the state of research in cutting dynamics. Ann CIRP

8. Wu DW (1989) A new approach of formulating the transfer function for dynamic cutting processes. J Eng Ind 111:37–47. https://doi.org/10.1115/1.3188730

9. Montgomery D, Altintas Y (1991) Mechanism of cutting force and surface generation in dynamic milling. J Eng Ind 113:160–168. https://doi.org/10.1115/1.2899673

10. Elbestawi MA, Ismail F, Du R, Ullagaddi BC (1994) Modelling machining dynamics including damping in the tool-workpiece interface. J Eng Ind 116:435–439. https://doi.org/10.1115/1.2902125

11. Chiou Y, Chung E, Liang S (1995) Analysis of tool wear effect on chatter stability in turning. Int J Mech Sci 37:391–404. https://doi.org/10.1016/0020-7403(94)00070-Z

12. Chiou RY, Liang SY (1998) Chatter stability of a slender cutting tool in turning with tool wear effect. Int J Mach Tools Manuf 38:315–327. https://doi.org/10.1016/S0890-6955(97)00079-5

13. Budak E, Tunc LT (2009) A new method for identification and modeling of process damping in machining. J Manuf Sci Eng 131. https://doi.org/10.1115/1.4000170

14. Ahmadi K (2017) Analytical investigation of machining chatter by considering the nonlinearity of process damping. J Sound Vib 393:252–264. https://doi.org/10.1016/j.jsv.2017.01.006

15. Tuysuz O, Altintas Y (2019) Analytical modeling of process damping in machining. J Manuf Sci Eng 141. https://doi.org/10.1115/1.4043310

16. Sims ND, Turner MS (2011) The influence of feed rate on process damping in milling: modelling and experiments. Proc Inst Mech Eng Part B J Eng Manuf 225:799–810. https://doi.org/10.1243/09544054JEM2141

17. Bachrathy D, Stepan G (2010) Time-periodic velocity-dependent process damping in milling processes. In: 2nd CIRP International Conference on Process Machine Interaction 06.10-06.11

18. Cao C, Zhang X-M, Ding H (2017) An improved algorithm for cutting stability estimation considering process damping. Int J Adv Manuf Technol 88:2029–2038. https://doi.org/10.1007/s00170-016-8884-x

19. Campomanes ML, Altintas Y (2003) An improved time domain simulation for dynamic milling at small radial immersions. J Manuf Sci Eng 125:416–422. https://doi.org/10.1115/1.1580852

20. Budak E, Tunc LT (2010) Identification and modeling of process damping in turning and milling using a new approach. CIRP Ann 59:403–408. https://doi.org/10.1016/j.cirp.2010.03.078